ANL/MSD/CP-96641

58930-00-105
58712-00-105
58918-00-105

Finite Element Modeling of the Effect of Interface Anomalies on Thermal Stresses in Alumina Scales

RECEIVED
SEP 28 1999
OSTI

J.K. Wright, R.L. Williamson

Idaho National Engineering and Environmental Laboratory
P.O. Box 1625, Idaho Falls, ID 83415-2218

P.Y. Hou, R.M. Cannon

Lawrence Berkeley Laboratory, Berkeley, CA 94720

D. Renusch, B. Veal, and M. Grimsditch

Materials Science Division, Argonne National Laboratory, Argonne, IL 60439

The submitted manuscript has been created by the University of Chicago as Operator of Argonne National Laboratory ("Argonne") under Contract No. W-31-109-ENG-38 with the U.S. Department of Energy. The U.S. Government retains for itself, and others acting on its behalf, a paid-up, nonexclusive, irrevocable worldwide license in said article to reproduce, prepare derivative works, distribute copies to the public, and perform publicly and display publicly, by or on behalf of the Government.

Proceedings of the 193rd Meeting of the Electrochemical Society, San Diego, CA, May 3-8, 1998

This work supported by the U.S. Department of Energy, Basic Energy Sciences-Material Sciences under contract No. W-31-109-ENG-38 at ANL and Nos. DE-AC07-91ID13223 and DE-AC-03-76F00098.

DISCLAIMER

This report was prepared as an account of work sponsored by an agency of the United States Government. Neither the United States Government nor any agency thereof, nor any of their employees, make any warranty, express or implied, or assumes any legal liability or responsibility for the accuracy, completeness, or usefulness of any information, apparatus, product, or process disclosed, or represents that its use would not infringe privately owned rights. Reference herein to any specific commercial product, process, or service by trade name, trademark, manufacturer, or otherwise does not necessarily constitute or imply its endorsement, recommendation, or favoring by the United States Government or any agency thereof. The views and opinions of authors expressed herein do not necessarily state or reflect those of the United States Government or any agency thereof.

DISCLAIMER

Portions of this document may be illegible in electronic image products. Images are produced from the best available original document.

FINITE ELEMENT MODELING OF THE EFFECT OF INTERFACE ANOMALIES ON THERMAL STRESSES IN ALUMINA SCALES

J. K. Wright and R. L. Williamson
Idaho National Engineering and Environmental Laboratory
P.O. Box 1625, Idaho Falls, ID 83415-2218

P. Y. Hou and R. M. Cannon
Lawrence Berkeley Laboratory
Berkeley CA 94720

D. Renusch, B. Veal and M. Grimsditch
Argonne National Laboratory
Argonne, IL 60439

The scales that grow from oxidation often develop a convoluted morphology or interface pores. High thermal stresses can develop locally and are potentially detrimental to the scale or interface integrity. Finite element simulations are used to examine residual thermal stresses and strains that result when these deviations from a flat interface have formed, and the resulting geometry is subsequently cooled to room temperature. A variety of geometries will be considered for alumina scales on a FeCrAl substrate.

INTRODUCTION

It has long been recognized that significant stress levels, which are often compressive, can develop in scales as a result of oxide growth (1). Compressive stresses, due to the thermal expansion mismatch of the oxide and the substrate, are presumably added during cooling, resulting in the total stress level. The magnitudes of these stresses and how they affect the scale growth and failure processes are important issues in understanding the protectiveness of the oxide scales.

The scales that grow from oxidation often develop a convoluted morphology as a result of the compressive stress in the oxide film. The convolution can be due to scale buckling, as in the case of many Cr_2O_3-forming alloys (2), where the scale detaches from the substrate and wrinkles under the influence of the in-plane compressive stress. It can also occur without any separation from the substrate, so that the scale and the scale/alloy interface corrugate together, giving rise to a wavy interface with fairly regular amplitude and wavelength distributions (3,4,5,6). Undoubtedly, one effect of such convolutions is a non-uniform stress distribution throughout the scale and near the interface in the

substrate. Although convolution relieves the overall growth stress, high thermal stresses can develop locally and can be detrimental to the scale or interface integrity. These stresses can cause interfacial void formation and spallation as presented by Suo (7) and discussed specifically for Al_2O_3 scales by Hou et al (8).

Most modeling studies to date have assumed that the interface is flat. Analytical solutions are available to describe the biaxial stress/strain conditions through the thickness of infinite plates of joined dissimilar linear-elastic or simple elastic-plastic materials (9,10). More complex nonlinear material behavior can be considered using simple finite element method (FEM) modeling (11,12,13,14,15,16). Recent FEM modeling of corners (17) has indicated that regions of local curvature can result in significant tensile stresses along the exterior surface of the oxide and large stress gradients in the scale as it bends in addition to contracting upon cooling. Evans et al (18) have provided some analytical solutions for the stresses along a sinusoidal interface for limiting cases, and recently this problem has been further studied using FEM (19, 20, 21, 22). Recently ruby fluorescence has been applied to measure the residual stress levels in thermally grown Al_2O_3 scales on FeCrAl across convolutions or near sample corners (23, 24). The technique can be performed with high spatial resolution, thus providing stress distributions at the micron scale and consequently the possibility of verifying model results.

In this investigation, finite element modeling is used to study the residual stresses and strains in a Fe-18Cr-5Al alloy that forms modestly adherent, convoluted or porous scales. The objectives of this research are to better understand surface oxide failure mechanisms, and ultimately to provide criteria for design of more adherent oxides.

MODELING

Approach

Finite element continuum models were used to compute the residual stresses and strains during simulated cooling from a stress free condition at 1000°C to ambient temperature in specimens where the oxide and substrate were assumed to be perfectly bonded. Stresses or deformation resulting from growth of the oxide were not considered; growth stresses are thought to be small relative to thermally generated stresses (3, 25). Cooling was assumed to be spatially uniform and relatively rapid, so time-dependent deformation (creep) was not considered, although the substrate was permitted to deform plastically. Numerical solutions were obtained with the ABAQUS finite element computer program (26) using a series of temperature decrements, with iteration within each decrement to obtain equilibrium. All simulations utilized second order (quadratic) elements.

The convolutions are assumed to have developed at the oxidation temperature (1000°C) and as a result are built into the model; development of the convoluted morphology was not considered (although the convolutions are free to further develop during cooling and do so to a very slight extent). Similarly, pores are assumed to have developed at the oxidation temperature, although additional cases where pores formed at an intermediate temperature of 500°C and after cooling to room temperature were also modeled.

Geometry and Computational Meshes

To simplify the complex specimen topography observed experimentally, convolutions are assumed to be sinusoidal in shape and to exist only in the x-y plane. The geometry consists of large convolutions alternating with small convolutions (Fig. 1), based on average ridge heights and widths determined from AFM line scans. Additional convoluted geometries have been presented elsewhere (21, 23). Meshes were refined near the material interface, especially in regions of large interface curvature (Fig. 2). Convolution modeling assumed generalized plane-strain, with constraints applied to force the front and back planes to remain parallel, thus simulating convolutions that extend into the plane of Fig. 2. Periodic boundaries were prescribed on the left and right sides of the mesh to simulate symmetric or repeating convolutions.

Three pore cross-sections were modeled at an interface: elliptical, football, and half-football (in the substrate only) (Fig. 3). Meshes were refined near the pore, especially in regions where the pores meet the interface (Fig. 4). Pore meshes utilized an axis of symmetry along the left side and a periodic boundary along the right side of Fig. 4, resulting in pores that are circular in plan view and centered in a large cylinder of material. To keep the models reasonably sized, substrate thicknesses were 50 times greater than the oxide layers for all geometries.

Material Behavior

All material properties, presented elsewhere (23), are assumed to be homogeneous and isotropic, and were obtained from tabulations for bulk materials. Temperature-dependent thermal expansion coefficients (27,28,29) are used for both materials. Elasticity properties (30), were assumed to be independent of temperature for the oxide since they are known to change less than 4% up to 1000°C (31), and to vary linearly for the FeCrAl (28). No plasticity effects were permitted in the scale. The temperature dependent yield strengths used for the alloy are based on data obtained for both FeCrAl and oxide (yttria) dispersion-strengthened (ODS) FeCrAlY (28). Because similar yield and ultimate tensile strengths for a wrought FeCrAlY, work hardening was not considered in the model.

RESULTS AND DISCUSSION

When a flat interface is cooled from oxidation to ambient temperature, it develops a state of biaxial stress ($\sigma_{xx}=\sigma_{zz}$, $\sigma_{yy}=0$) with the scale in biaxial compression and the substrate in biaxial tension because of the difference in thermal contraction of the two materials. If no bending of the substrate occurs, there are no significant stress gradients in either the coating or substrate except near edges or corners.

Convolutions

When a scale has interface convolutions, localized bending results. As the scale is placed in compression during cooling, the convolutions steepen, and the scale at each peak behaves similarly to an elastic beam in bending, with tensile stresses present along the outside of the beam and compressive stresses on the inside. As a result, the residual stresses are no longer biaxial but contain significant gradients. Stresses in the scale are analogous to those observed in a simple corrugated beam placed in axial compression, but are not symmetrical (i.e. the stresses at point A of Fig. 1 are not the same as those at point D, and the stresses at point B do no equal those at point C) because of the constraint provided by the substrate.

Figures 5a and b show computed contours of the σ_{xx} and σ_{yy} stress components, respectively (refer to Fig. 1 for component notation) in the scale/interface region after cooling to room temperature. Tensile σ_{xx} stresses occur at the outside of the large peak (point A), and compressive σ_{xx} stresses inside bends (points B and C). Such stresses obviously lead to large σ_{xx} gradients through the scale thickness. Interestingly, the maximum σ_{xx} tensile stress in the scale is not at the spatial peak in the convolution, but occurs at the surface, a short distance from the peak. The σ_{yy} component, which is zero for a flat interface, is significant for the convoluted geometry with the largest tensile values occurring near the interface in the vicinity of a peak (point B), especially in the substrate. Note the difference in stress magnitudes between Fig. 5a and b; the σ_{xx} compressive stresses are nearly an order of magnitude larger than the σ_{yy} compressive stresses, but the σ_{xx} tensile stresses are about half of the σ_{yy} tensile stresses. Computed contours of the hydrostatic stress, the stress invariant used for comparison with ruby fluorescence measurements, are shown in Fig. 5c. Note that all hydrostatic stresses in the scale are compressive. The hydrostatic stress computed for a bonded infinite plate geometry of the two materials, i.e. the theoretical hydrostatic stress of a flat scale of the same thickness, σ_H^{∞}, is -2.19 GPa.

Contours of the equivalent plastic strain[1] are shown in Fig. 6. Peak strains are significant in magnitude, over 1%, and extend to depths comparable to the scale thickness. Plastic strain accumulates throughout the cooling process; at high temperatures thermal strains are low but so is the yield strength of the substrate, while at low temperatures the opposite is true, supporting the necessity of including temperature-dependent plasticity, in contrast to previous work (22). In the substrate, beneath the peak (point B), the horizontal plastic strain component (ε^p_{xx}) is compressive and the vertical component (ε^p_{yy}) tensile. The inverse is true under each valley. This strain pattern leads to a steepening of the substrate convolution during cooling as substrate material from the valley region flows up into the area under the peak.

Verification of model results are provided by comparing the hydrostatic stress of the oxide, with ruby fluorescence measurements of convoluted alumina/FeCrAl interfaces as a function of specimen position, in Fig. 7. The comparison was made by averaging σ_H across the volume of several columns of elements to achieve an approximate excited volume of 1 μm^3 at both peaks, the midpoint and the valley. This volume was based on a 1 μm diameter spot through the 1 μm scale thickness, since the oxides are relatively transparent and the entire scale thickness is probed experimentally. Further details of the sample preparation and stress measurement technique are presented elsewhere (23, 24).

Agreement of computed volume averaged results with the measured data is very good; both the shape of the curves and the stress magnitudes in Fig. 7 are similar. The small offset between the model curve and experimental data suggests that while growth stresses are large enough to cause convolutions to form at the oxidation temperature, this process has relaxed them and they are minimal compared to the thermally generated stresses present at room temperature (25). Agreement between model and experiment also suggests that the geometrical simplifications required for modeling, i.e. parallel ridges (modeling in 2D plane strain) with sinusoidal cross-sections of average width and height, are reasonable.

Pores

When a pore forms, the interface is locally free of the constraints that typically result from the material present when no pore exists. As the scale is placed in compression during cooling, the side of the pore moves toward the center of the pore, causing slightly compressive σ_{xx} in the otherwise tensile substrate below the pore, and an increased compressive σ_{xx} and σ_{yy} in the scale above the pore (Fig. 8). Elevated compressive stresses above the pore increase the potential for scale buckling, particularly as the size of the pore is increased and the stresses presumably increase as well.

---

[1] The equivalent plastic strain is defined as $(2/3\ \varepsilon^p:\varepsilon^p)^{1/2}$ where $\varepsilon^p:\varepsilon^p$ is the scalar product of the plastic strain tensor.

Where the material interface intersects the pore, significant local tensile stresses can be seen for both the σ_{xx} and σ_{yy} components in Fig. 8. However, a stress singularity forms at this location during cooling, as in the case of any dissimilar material interface that meets a free surface. Because of the singularity, results very near this point are not quantitatively reliable, but should be reliable at a distance of about two elements in any direction (32), hence the very refined mesh in this region.

Fig. 9a shows the equivalent plastic strain where the interface meets the elliptical pore. Strains are significant in magnitude (6.5% at the third element in from the pore edge). However, plasticity is very localized, with a plastic zone size[2] of only 0.084 μm, less than half the length of the pore. Stress profiles for a purely elastic substrate generate identical stress profiles to that of a perfectly plastic substrate, except very near the singularity, where the elastic calculation yields larger stresses, further illustrating the very local effect of plasticity.

The primary differences between the elliptical and football shaped pores result from differences in the equivalent plastic strain (Fig. 9). The maximum strain magnitudes appear to be higher (8.2% at the third element in from the pore edge), but the plastic zone size is smaller (0.064 μm), indicating that the vertex creates a more severe stress concentration, as expected. The football pore also has somewhat higher compressive σ_{xx}, σ_{yy} and σ_{xy} in the scale above the pore, indicating a higher potential for scale buckling and subsequent delamination.

In contrast to pores intersecting the interface, when the pore forms only in the substrate, stress profiles deviate relatively little from the biaxial condition and no plastic strain is observed. The scale above the pore effectively constrains the edge of the pore from displacing significantly towards its center. This may not be the case when the scale above the pore is curved, as when a pore forms under the peak of a convolution (7).

Interestingly, the temperature at which the pore forms has little effect on the magnitude of the plastic strain observed. When the pore was formed at the oxidation temperature of 1000°C, plastic strains form in the substrate as it cools. If the material cools first, the biaxial thermal stresses generated are not sufficient to cause plastic strain, but once the pore forms at room temperature, the stresses redistribute as equilibrium is achieved, and plastic strain develops. Similarly, when the pore forms at an intermediate temperature, no plastic strains form during initial cooling to 500°C, but develops both as the pore forms, and during subsequent cooling to room temperature. In all three cases, the maximum stress in the third element is about 8%. However, the plastic zone size is somewhat larger when the pore forms at 1000°C (0.064 μm compared to 0.036 μm when the pore forms at either 500°C or at room temperature).

---

[2] The distance along the interface where equivalent plastic strains are greater than zero.

CONCLUSIONS

Residual stresses in the convoluted alumina scale on a FeCrAl alloy have been measured using ruby fluorescence and modeled using FEM. Good agreement was found between the two methods, with both showing a systematic variation in stress between peak and valley locations. While the hydrostatic stresses are compressive throughout the scale, modeling indicates local tensile stress components in the peak of convolutions both near the free surface and the interface.

Interface pores result in increased compressive stresses in the scale above the pore. Although a stress singularity forms where the interface intersects the edge of the pore, FEM modeling can provide useful information near, but not at this singularity. Differences between various pore geometries and substrate plasticity assumptions arise from very localized differences in plastic strain. The temperature at which the pore forms, for the pore geometries considered in this study, only minimally affects plastic strain behavior.

Anomalous geometries at the interface, such as convolutions and pores, cause stress gradients in an otherwise biaxial stress distribution. The FEM analysis provides detailed information about all stress and strain components, plasticity effects, and gradients, and proves very useful in providing an increased understanding of the complex mechanical response in interface anomalies during cooling. However, to be truly useful, the simplifications and assumptions regarding geometry and material properties that must be implemented in order to carry out the FEM require experimental verification.

ACKNOWLEDGMENTS

The U.S. Department of Energy, Office of Energy Research, Office of Basic Energy Sciences, Materials Science Division, supported the work described in this paper under 33Contract Nos. DE-AC07-94ID13223, DE-AC03-76F00098, and W-31-109-ENG-38.

REFERENCES

1. See for examples, J. Stringer, Corr. Sci., **10**, 513 (1970).
2. P. Kofstad, High Temperature Corrosion, Elsevier Applied Science (1988).
3. P. Y. Hou and J. Stringer, J. de Physique IV, **3**, 231 (1993).
4. P. Fox and G. J. Tatlock, Mater. Sci. Engr., **4**, 439 (1988).

5. V. K. Tolpygo and H. J. Grabke, Oxid. Metals, **41**, 343 (1994).

6. M. C. Stasik, F. S. Pettit, G. H. Meier, A. Ashary and J. L. Smialek, Scripta Metall., **31**, 1645 (1994).

7. Z. Suo, J. Mech. Phys. Solids, **43**, 829 (1995).

8. P. Y. Hou, R. M. Cannon, H. Zhang and R. L. Williamson, in Fundamental Aspects of High Temperature Corrosion/1996, D. A. Shores, R. A. Rapp and P. Y. Hou , Editors, p. 28, Electrochem. Society Proceedings., Pennington, PA, (1997).

9. C. H. Hsueh and A. G. Evans, J. Am. Ceram. Soc., **68**, 241 (1985).

10. T. Yada and H. Koguchi, JSME Int. J., **34**, 163 (1991).

11. H. C. Cao, M. D. Thouless, and A. G. Evans, Acta Metall., **36**, 2037 (1988).

12. R. O. Ritchie, R. M. Cannon, B. J. Dalgleish, R. H. Dauskardt, and J. M. McNaney, Mater. Sci. Engr., **A166**, 221 (1993).

13. M. Y. He, A. G. Evans, and J. W. Hutchinson, Int. J. Solids Struct., **31**, 3443 (1994).

14. H. Kobayashi, Y. Arai, H. Nakamura and T. Sato, Mater. Sci. Engr., **A143**, 91 (1991).

15. B. E. Sheets and K. Kokini, Compos. Mater. Tech. ASME, **37** (1991) 257.

16. H. E. Evans, G. P. Mitchell, R. C. Lobb and D. R. J. Owen, Proc. R. Soc. Lond., **A440**, 1 (1993).

17. J. K. Wright, R. L. Williamson, and R. M. Cannon, Mater. Sci. Engr. **A238**, 411 (1997).

18. A. G. Evans, G. B. Crumley and R. E. Demaray, Oxid. Metals, **20**, 193 (1983).

19. G. C. Chang, W. Phucharoen, and R. A. Miller, Surface and Coatings Technology, **32**, 307 (1987).

20. G. Petrus and B. L. Ferguson, in Thermal Barrier Coating Workshop, NASA Conference Publication 3312, p. 251, Proceedings of a conference held at NASA Lewis Research Center, Cleveland, OH (1995).

21. R. L. Williamson, J. K. Wright and R. M. Cannon, in Fundamental Aspects of High Temperature Corrosion/1996, D. A. Shores, R. A. Rapp and P. Y. Hou , Editors, Electrochem. Society Proceedings., Pennington, PA, (1997).

22. J. Chao and J. L. González-Carrasco, Mater. Sci. Engr., **A230**, 39 (1997).

23. J. K. Wright, R. L. Williamson, D. Renusch, B. W. Veal, M. Grimsditch, P. Y. Hou and R. M. Cannon, submitted to Mater. Sci. Engr. A.

24. M. Grimsditch, D. Renusch, B. W. Veal, J. K. Wright and R. L. Williamson in this proceedings, The Electrochemical Society, Pennington, NJ (1998).

26. ABAQUS computer code, Hibbitt, Karlsson and Sorensen, Inc., Providence, RI (1997).

27. Thermophysical Properties of Matter: Volume 13, Y. S. Touloukian, R. K. Kirby, R. E. Taylor and T. Y. Lee, Editors, Thermal Expansion Nonmetallic Solids, Plenum, New York, (1977).

28. Metals Handbook, 10th ed., Volume 2 Properties and Selection: Nonferrous Alloys and Special Purpose Materials, pp. 823-827, ASM International, Metals Park, OH (1990).

29. Plansee, Metallwerk Plansee GmbH/Lechbruck, PM ODS Werkstoffe, Material Data Sheet ODS - Superalloy PM2000 (1993).

30. W. J. Lackey, D. P. Stinton, G. A. Cerny, L. L. Fehrenbacher and A. C. Schaffhauser, in Ceramic Coatings for Heat Engine Materials - Status and Future Needs, Oak Ridge National Laboratory Report ORNL/TM-8959 (1984).

31. E. Zouboulis and M. Grimsditch, J. Applied Physics, 70, 772 (1991).

32. J. D. Whitcomb, I. S. Raju and J. G. Goree, Computers and Structures, 15, 23 (1982).

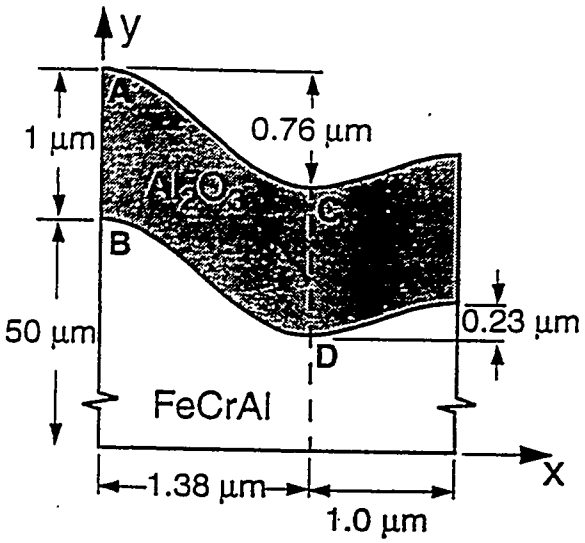

Fig. 1. Schematic of convolution geometry.

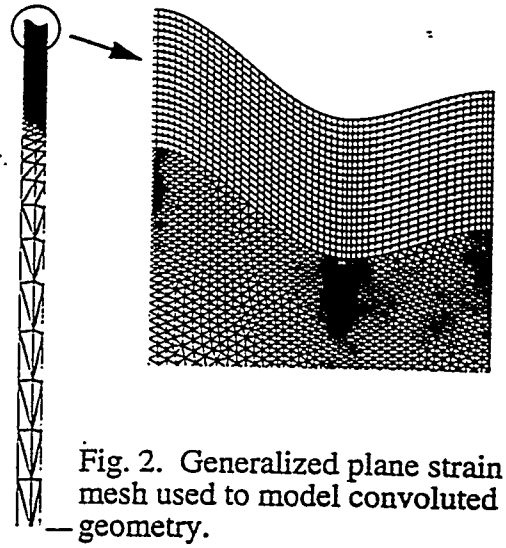

Fig. 2. Generalized plane strain mesh used to model convoluted geometry.

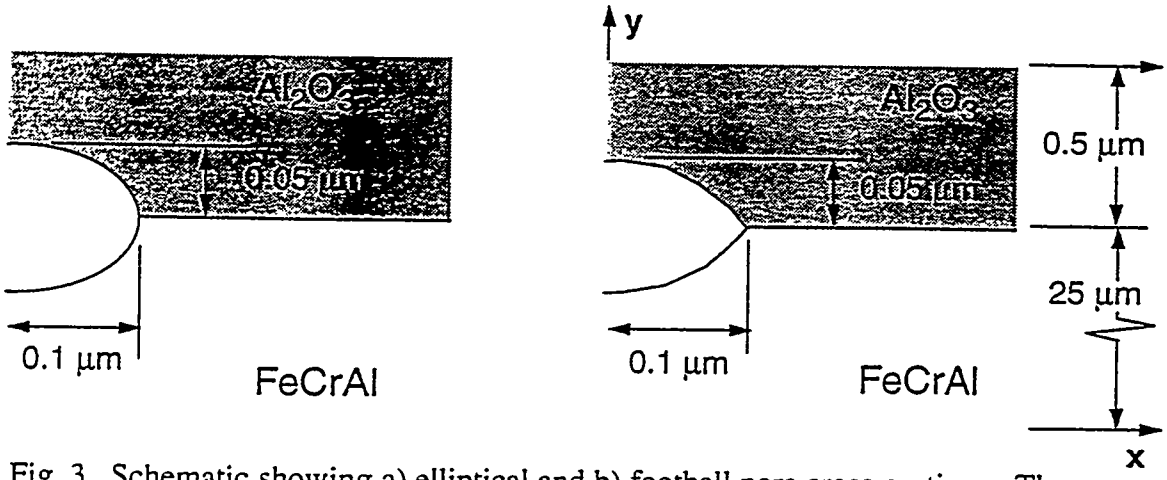

Fig. 3. Schematic showing a) elliptical and b) football pore cross-sections. The half-football pore is like b, but in the substrate only.

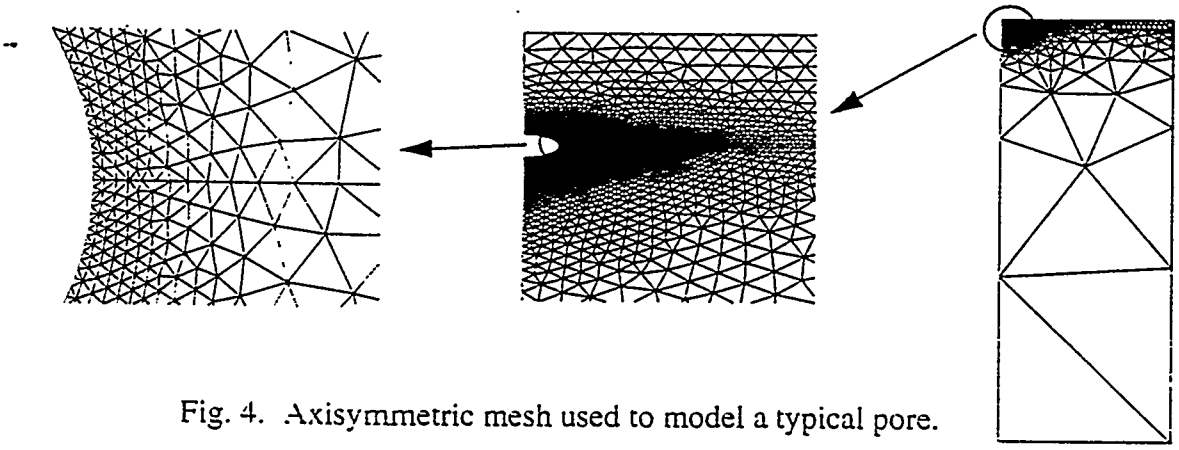

Fig. 4. Axisymmetric mesh used to model a typical pore.

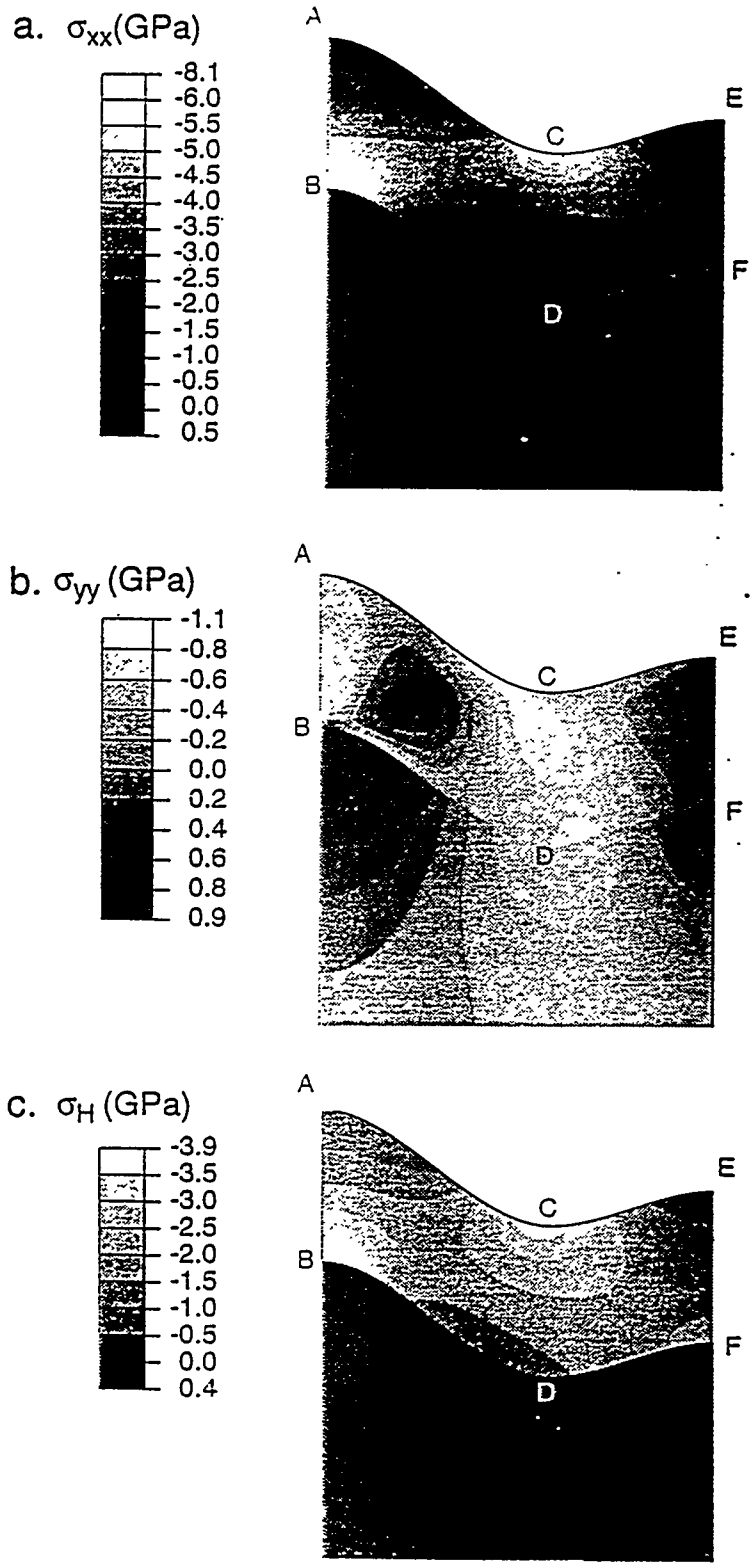

Fig. 5. Stress contours for the convoluted interface: a)σ_{xx}, b) σ_{yy}, and c) hydrostatic stress.

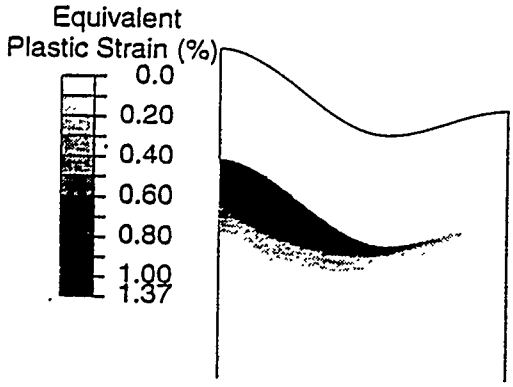

Fig. 6. Equivalent plastic strain contours for the convoluted interface.

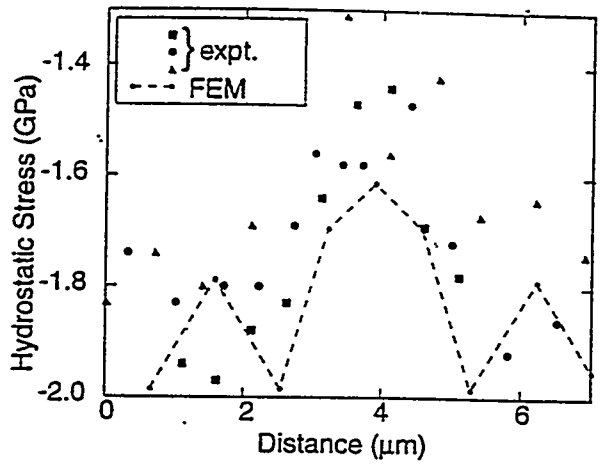

Fig. 7. Comparison of experimentally determined and modeled hydrostatic stress. FEM data hasbeen reflected across the model planes of symmetry and lines are provided for clarity.

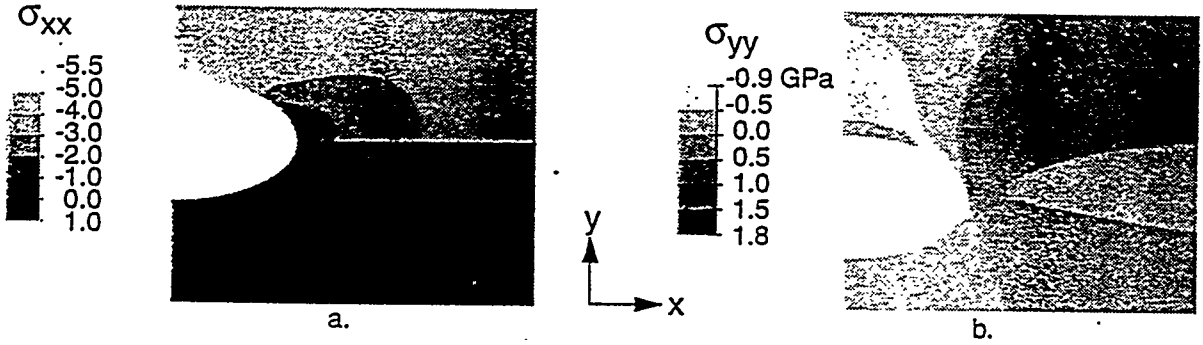

Fig. 8. Stress contours for the elliptical pore; a) σ_{xx} and b) σ_{yy}.

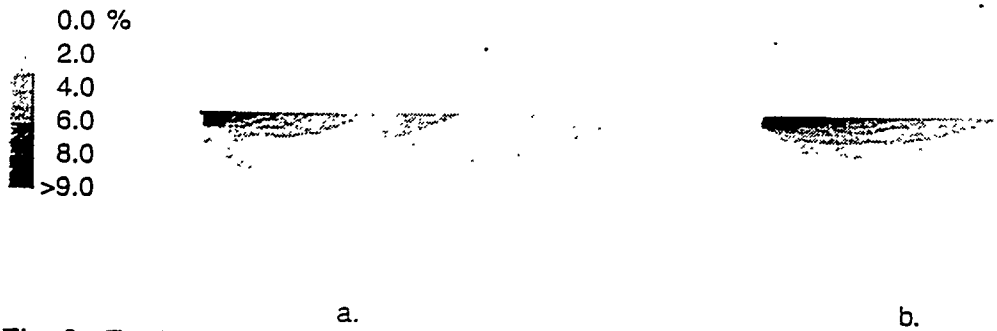

Fig. 9. Equivalent plastic strain contours for a) the elliptical and b) the football pore.